Brain, Behavior, and Immunity 121 (2024) 1–12

Contents lists available at ScienceDirect

Brain Behavior and Immunity

journal homepage: www.elsevier.com/locate/ybrbi

Full-length Article

Transcriptomic and proteomic profiling of bi-partite and tri-partite murine iPSC-derived neurospheroids under steady-state and inflammatory condition

Julia Di Stefano [a,b], Laura Garcia-Pupo [a,c], Federica Di Marco [d,e], Helena Motaln [f], Jonas Govaerts [a], Elise Van Breedam [a], Ligia Monica Mateiu [g], Siebe Van Calster [a], Leonardo Ricciardi [a,b,h], Alessandra Quarta [a], Peter Verstraelen [h,i], Winnok H. De Vos [h,i], Boris Rogelj [f], Ilaria Cicalini [d,e], Vincenzo De Laurenzi [d,e], Piero Del Boccio [d,j], Una FitzGerald [k,l], Wim Vanden Berghe [c], Marleen Verhoye [b,h], Damiana Pieragostino [d,e], Peter Ponsaerts [a,*]

[a] Laboratory of Experimental Hematology, Vaccine and Infectious Disease Institute (Vaxinfectio), University of Antwerp, 2610 Wilrijk, Belgium
[b] Bio-Imaging Lab, University of Antwerp, 2610 Wilrijk, Belgium
[c] Cell Death Signaling, Integrated Personalized and Precision Oncology Network (IPPON), University of Antwerp, 2610 Wilrijk, Belgium
[d] Center for Advanced Studies and Technology (CAST), G. d'Annunzio University of Chieti-Pescara, 66100 Chieti, Italy
[e] Department of Innovative Technologies in Medicine and Dentistry, University "G. d'Annunzio" of Chieti-Pescara, 66100 Chieti, Italy
[f] Department of Biotechnology, Jozef Stefan Institute, SI-1000 Ljubljana, Slovenia
[g] Center for Medical Genetics, Faculty of Medicine and Health Sciences, Antwerp University Hospital, University of Antwerp, Edegem, Belgium
[h] μNEURO Research Centre of Excellence, University of Antwerp, 2610 Wilrijk, Belgium
[i] Laboratory of Cell Biology and Histology and Antwerp Center for Advanced Microscopy, Department of Veterinary Sciences, University of Antwerp, 2610 Wilrijk, Belgium
[j] Department of Pharmacy, G. d'Annunzio University of Chieti-Pescara, 66100 Chieti, Italy
[k] CÚRAM, Centre for Research in Medical Devices, Biomedical Engineering, University of Galway, Ireland
[l] Galway Neuroscience Centre, University of Galway, Ireland

ARTICLE INFO

Keywords:
Murine iPSC
Neurospheroids
Microglia
Inflammatory response
Stress granules
Transcriptomics
Proteomics

ABSTRACT

induced-pluripotent stem cell (iPSC)-derived neurospheroid (NSPH) models are an emerging *in vitro* toolkit to study the influence of inflammatory triggers on neurodegeneration and repair in a 3D neural environment. In contrast to their human counterpart, the absence of murine iPSC-derived NSPHs for profound characterisation and validation studies is a major experimental research gap, even though they offer the only possibility to truly compare or validate *in vitro* NSPH responses with *in vivo* brain responses. To contribute to these developments, we here describe the generation and characterisation of 5-week-old $CX_3CR1^{eGFP+/-}$ $CCR2^{RFP+/-}$ murine (m)iPSC-derived bi-partite (neurons + astrocytes) and tri-partite (neurons + astrocytes + microglia) NSPH models that can be subjected to cellular activation following pro-inflammatory stimulation. First, cytokine analysis demonstrates that both bi-partite and tri-partite NSPHs can be triggered to release IL6 and CXCL10 following three days of stimulation with, respectively, TNFα + IL1β + IFNγ and LPS + IFNγ. Additionally, immunocytochemical analysis for G3BP1 and PABPC1 revealed the development of stress granules in both bi-partite and tri-partite NSPHs after 3 days of stimulation. To further investigate the observed signs of inflammatory response and cellular stress, we performed an untargeted transcriptomic and proteomic analysis of bi- and tri-partite NSPHs under steady-state and inflammatory conditions. Here, using the combined differential gene and protein expression profiles between unstimulated and stimulated NSPHs, Ingenuity Pathway Analysis (IPA) confirms the activation of canonical pathways associated with inflammation and cellular stress in both bi-partite and tri-partite NSPHs. Moreover, our multi-omics analysis suggests a higher level of downstream inflammatory responses, impairment of homeostatic and developmental processes, as well as activation of cell death processes in stimulated tri-partite NSPHs compared to bi-partite NSPHs. Concluding, these results emphasise the advantages

* Corresponding author.
E-mail address: peter.ponsaerts@uantwerpen.be (P. Ponsaerts).

https://doi.org/10.1016/j.bbi.2024.07.008
Received 5 March 2024; Received in revised form 24 May 2024; Accepted 6 July 2024
Available online 14 July 2024

of including microglia in NSPH research to study inflammation-induced neurodegeneration in a 3D neural environment.

1. Introduction

Neuroinflammation is a common feature of many neurological disorders, whose main players are activated microglia, astrocytes and infiltrating peripheral immune cells. Such neuroinflammatory processes are characterized by an increased release of pro-inflammatory cytokines and chemokines, reactive oxygen species and secondary messengers, all potentially leading to loss of cellular homeostasis, developmental processes and cell viability (DiSabato et al., 2016). Despite decades of neuroinflammatory research and thousands of potential disease-modifying therapies suggested, to date treatment and/or restoration of inflammation-mediated neurological disorders remains a major challenge. From an experimental point of view, the study of neuroinflammation, as well as the pre-clinical validation of novel immune-modulatory and regeneration-inducing therapies, is commonly performed in rodent animal models. Given the world-wide recognition that efforts should be made to reduce animal experiments for ethical, scientific and practical reasons, there is an unmet need for the development and validation of novel pre-clinical screening tools before moving towards animal studies and/or human clinical trials. In this context, immune-competent 3D neural models, such as organoids and spheroids, are biologically more relevant as compared to classical 2D cell (co–) cultures models in terms of approaching the more complex *in vivo* neural environment. As such, there is compelling evidence that NSPHs outperform 2D cell co-cultures in terms of 3D architecture, cell heterogeneity, cell–cell interactions, gene expression, phenotypic profile, response to inflammatory stress and drug response (Lancaster et al., 2014). Over the past decade, a large number of studies using immune-competent human iPSC-derived brain organoids were published. In brief, they covered pharmacological studies (Renner et al., 2020; Fan et al., 2022) or disease modelling, such as Alzheimer's disease and/or neuroinflammation (Abud et al., 2017; Lin et al., 2018; Jin et al., 2022), Parkinson's disease (Sabate soler et al., 2022), Zika virus (Xu et al., 2021; Abreu et al., 2018; Muffat et al., 2018) and SARS-CoV-2 infection (Samudyata et al., 2022). In these studies, the inflammatory processes were mainly characterised by means of microglia morphological analysis, immunocytochemical analyses of phagocytosis, cytokine release profiling and in some cases by RNA-sequencing (Abud et al., 2017; Sabate Soler et al., 2022; Samudyata et al., 2022). Nevertheless, it is clear that profound NSPH analysis, including deep phenotypic and functional profiling, will require an extensive and complementary toolbox including real-time imaging, electrophysiology, transcriptomics, proteomics and metabolomics. To develop such pipelines, especially considering the culture time and associated costs for generating immune-competent hiPSC-derived NSPHs, immune-competent miPSC-derived NSPHs may be a fast and cost-effective alternative to provide proof-of-concept for novel analytical approaches.

However, in contrast to the growing number of immune-competent hiPSC-derived NSPH models, there are currently no well-characterised protocols for the generation of immune-competent miPSC-derived NSPH models. Nevertheless, such models are a great complement to currently unavoidable rodent studies. In this study, we optimised culture conditions for the generation of miPSC-derived bi-partite and tri-partite NSPH models that can be subjected to cellular activation following pro-inflammatory stimulation, as demonstrated by cytokine production and the formation of stress granules. In order to provide a broader picture of the cellular processes activated in immune-stimulated bi- and tri-partite NSPHs, untargeted transcriptomic and proteomic analyses were performed under steady-state and inflammatory conditions. The integrative multi-omics analysis presented will now pave the way for future affordable and scalable studies on inflammation-mediated neurodegeneration, protection and repair using immune-competent miPSC-derived NSPHs.

2. Materials and Methods

2.1. Generation of iPSC-derived embryoid bodies, bi-partite and tri-partite NSPHs

All media and cell culture supplements were purchased from Thermo Fisher Scientific, unless otherwise specified. All cell cultures were performed at 37 °C in a standard humidified cell culture incubator with 5 % CO_2. Embryoid bodies (EBs), bi-partite NSPHs and tri-partite NSPHs were generated starting from a previously established and validated C57BL/6 $CX_3CR1^{eGFP+/-}$ $CCR2^{RFP+/-}$ murine iPSC line cultured on mitotically inactivated mouse embryonic fibroblasts in standard murine "iPSC medium", as described in detail in preceding studies (Quarta et al., 2019 & 2021). EB and NSPH cultures were initiated starting from $2x10^3$ iPSC seeded per well in U-shaped 96-well plates in 100 μL of specific culture medium, as specified below. To allow for proper spheroid formation, plates were first treated with anti-adherence rinsing solution (Stemcell Technologies) for one hour at room temperature and subsequently washed three times with 1X phosphate-buffered saline (PBS) before seeding the iPSC. All spheroid cultures were maintained in the incubator under constant orbital shaking (88 rpm). To generate EBs (Fig. 1A), seeded iPSC were cultured in "EB medium", composed of DMEM/F12 medium and Neurobasal-A medium (at a 1:1 ratio), supplemented with 20 % foetal bovine serum (FBS), 0,5 % N2 supplement (Gibco), 1 % B27 supplement (Gibco) and 100 U/mL–100 μg/mL penicillin–streptomycin (Gibco). Two days after plating the iPSCs, 100 μL of fresh medium was added followed by a half medium change every other day until the EBs had reached the age of 3 weeks, after which they were processed for immunocytochemical analysis (ICC). For the generation of bi-partite NSPHs (Fig. 1B), the seeded iPSCs were cultured in neural differentiation medium ("ND medium"), composed of DMEM/F12 medium and Neurobasal-A medium (at a 1:1 ratio), supplemented with 0,5 % N2 supplement (Gibco), 1 % B27 supplement (Gibco) and 100 U/mL–100 μg/mL penicillin–streptomycin (Gibco). Two days after plating the iPSCs, 100 μL of fresh medium was added after which a half medium change was performed every second day until the bi-partite NSPHs had reached the age of 4,5 weeks for further experiments. For the generation of tri-partite NSPHs (Fig. 1C), the same procedure was followed as for bi-partite NSPHs with the following two exceptions: (i) after two weeks of culture, $2x10^4$ microglia progenitor (MP) cells were added to the NSPH cultures, and (ii) between week 4 and week 4,5 the ND medium was replaced with a 3:1 ratio of ND medium and microglia differentiation medium 1 (MD medium 1, see below). At 4,5 weeks, the medium was changed to ND medium and tri-partite NSPHs were used for further experiments.

2.2. Generation of murine iPSC-derived microglia progenitor cells

Murine iPSC-derived MP cells (Fig. 1D) were generated from $CX_3CR1^{eGFP+/-}$ $CCR2^{RFP+/-}$ iPSCs according to our previously reported protocol (Quarta et al., 2019). Briefly, $6x10^5$ iPSCs were seeded in an agarose-coated (Fisher-Scientific) 10 cm Petri dish in MD medium 1, composed of GMEM medium (Sigma-Aldrich) supplemented with 10 % FBS, 2 mM L-glutamine, 1 mM sodium pyruvate, 0,05 mM β-mercaptoethanol, 1 × MEM Non-Essential Amino Acids (NEAA) solution and 100 U/mL–100 μg/mL penicillin streptomycin. Following 8 days of culture, with a single medium change at day 4, cell aggregates were collected and transferred to a gelatine-coated (Sigma-Aldrich) T175

flasks in MD medium 1^+, composed of MD medium 1 additionally supplemented with 100 ng/mL murine stem cell factor (ImmunoTools) and 5 ng/mL murine vascular endothelial growth factor-A (ImmunoTools). On day 11, MD medium 1^+ was replaced by microglia differentiation medium 2 (MD medium 2), composed of MD medium 1 supplemented with 1 ng/mL murine IL3 (ImmunoTools), 20 ng/mL murine granulocyte–macrophage colony stimulating factor (GM-CSF; ImmunoTools), 15 % (vol/vol) L929-derived conditioned medium (CM) and 20 % (vol/vol) bEnd5-derived CM, with one medium change on day 13. From day 15 of differentiation, cultures were maintained solely in MD medium 1, after which microglia progenitor cells were spontaneously released into the culture supernatant. Medium was changed weekly, and microglia progenitor cells were collected starting from day 21 of differentiation for addition to the two-week-old NSPHs to generate the tri-partite NSPHs.

2.3. NSPH size measurements

The diameter of NSPHs was measured every week for 5 weeks using a Fluovert Leitz microscope and the CellSens Entry v.2.1 software.

2.4. Inflammatory stimulation of bi-partite and tri-partite NSPHs

At the age of 4,5 weeks, individual bi- and tri-partite NSPHs were stimulated in 200 µl ND medium with single or combined pro-inflammatory stimuli at the following final concentrations: 1 µg/mL Lipopolysaccharide (LPS; Sigma), 50 ng/mL interferon-γ (IFNγ; ImmunoTools), 10 ng/mL tumour necrosis factor alpha (TNFα; Abcam), 10 ng/mL interleukin 1 beta (IL1β; Biotechne). After 72 h, culture supernatant of unstimulated and stimulated NSPHs was collected and frozen for further cytokine analysis. Unstimulated and stimulated NSPHs were further processed for ICC, transcriptomic and proteomic analysis, as described in detail below.

2.5. Cytokine production by stimulated bi-partite and tri-partite NSPHs

Concentrations of interleukin 6 (IL6) and C-X-C motif chemokine ligand 10 (CXCL10) in cell culture supernatant were determined using commercially available ELISA kits (BioLegend and Biotechne, respectively), according to the manufacturer's instructions.

2.6. Immunocytochemical stainings

EBs, bi-partite and tri-partite NSPHs were individually fixed in 1,5 mL of 4 % paraformaldehyde solution in PBS in 2 mL microtubes at RT for 30 min. Following two wash steps with 1,5 mL of PBS, spheroids were stored at 4 °C in PBS containing sodium azide. Next, spheroids were processed for cryosectioning as previously described (Van Breedam et al., 2022). Ten µm thick frozen fixed sections were collected on glass slides coated with poly-L-lysine (Sigma), air-dried and stored at −20 °C before further processing. For immunofluorescence labelling, sections were re-hydrated with PBS for 20 min, permeabilized with 0,1% (v/v) Triton X-100 (Sigma) in Tris-buffered saline (TBS) for 30 min and blocked with 20 % serum (of the appropriate secondary antibody host species) or 1 % BSA in TBS for 1 h. Sections were incubated overnight at 4 °C with primary antibodies. After washing with TBS and a subsequent 1-hour incubation with the secondary antibodies in the dark, slides were washed again and counterstained with DAPI (1 µg/ml, Sigma) for 10 min at 4 °C. After a final washing step with distilled water, sections were mounted in ProLong R Gold antifade reagent (Thermo Fisher). The following antibody combinations were used in this study: a mouse anti-βIIItubulin primary antibody (Biotechne, MAB1195, 1:250) in combination with an Alexafluor 555-labeled goat anti-mouse secondary antibody (Invitrogen, A21425, 1:200), a rabbit anti-GFAP primary antibody (Abcam, ab7260, 1:1000) in combination with a Texas red-labelled goat anti-rabbit secondary antibody (Abcam, ab6719, 1:400), a mouse anti-G3BP1 monoclonal primary antibody (Proteintech, 66486–1-Ig, 1:500) in combination with an Alexafluor 555-labelled goat anti-mouse secondary antibody (Invitrogen, A21127, 1:1000), a rabbit anti-PABPC1 polyclonal antibody (Proteintech, 10970-1AP, 1:100) in combination with either an Alexafluor 488-labelled donkey anti-rabbit secondary antibody (Invitrogen, A21206, 1:1000) or an Alexafluor 647-labelled goat anti-rabbit secondary antibody (Invitrogen, A21245, 1:1000), a guinea pig anti-synaptophysin polyclonal antibody (Synaptic Systems, 101–004, 1:2000) in combination with a Cy3-labelled donkey anti-guinea pig secondary antibody (Jackson ImmunoResearch, 706–165–148, 1:500).

2.7. Microscopy and image analysis

Live images of bi-partite and tri-partite NSPHs were captured with a Zeiss Observer Z1 microscope. Immunofluorescence images of stained EBs, bi-partite and tri-partite NSPHs were acquired using a BX51

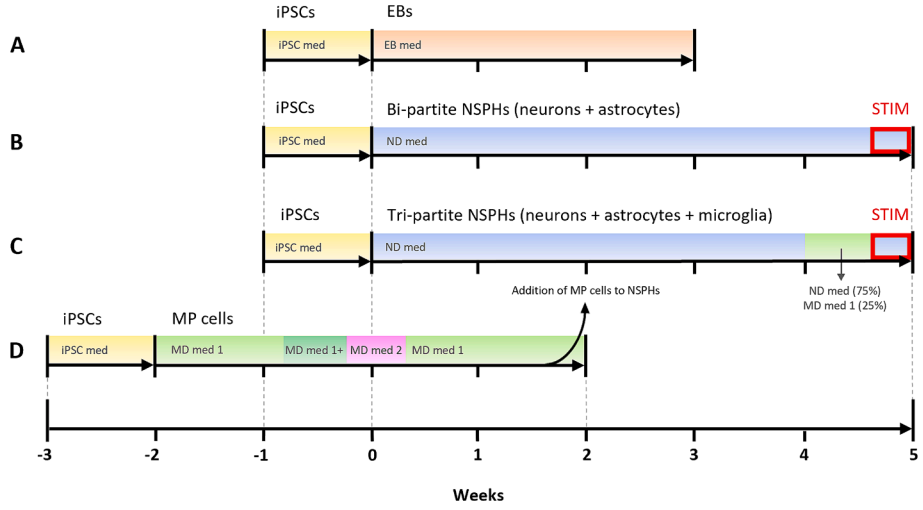

Fig. 1. Generation of murine iPSC-derived EBs, bi-partite and tri-partite NSPHs. Schematic outline of the murine iPSC differentiation protocols used to generate EBs, bi-partite and tri-partite NSPHs, indicating the timing and media composition during the different stages of differentiation and stimulation. Abbreviations: iPSC, induced pluripotent stem cells; med, medium; EB, embryoid body; NSPH, neurospheroid; ND, neural differentiation; MD, microglia differentiation; MP, microglia progenitor; STIM, stimulation.

fluorescence microscope equipped with an Olympus DP71 digital camera and using a 10× (NA 0,30), 20× (NA 0,50) or 40× (NA 0,75) dry objective. High-resolution images were acquired using the Nikon CSU-W1 SoRa confocal microscope with 40× (water) objective in normal confocal mode and NIS-Elements software (Nikon) and the Nikon CSU-W1 spinning disk confocal microscope with 40× (dry, NA 0.95 or water, NA 1.15) objectives, Kinetix sCMOS camera (Teledyne Photometrics) and NIS-Elements software (Nikon). All stainings were performed at least three times on multiple EBs or NSPHs. Representative images were selected and presented in this manuscript.

2.8. Data representation and statistical analysis

Dot plots representing NSPH growth and cytokine production were created with GraphPad Prism v.8.2.1 software. Statistical analysis was carried out using GraphPad Prism. For NSPH growth, a Kruskal-Wallis analysis was performed with Dunn's post-hoc correction comparing each time point to the 3rd week. For cytokine production by bi-partite NSPHs, a Kruskal-Wallis analysis was performed with Dunn's post-hoc correction following comparison of each stimulated condition with the unstimulated control. For cytokine production by tri-partite NSPHs, a MWU test was performed comparing the stimulated condition with the unstimulated control. A p-value $< 0,05$ was considered statistically significant. All other statistical analyses were performed with IPA.

2.9. RNA sequencing

Following collection of the cell culture supernatant, individual bi- and tri-partite NSPHs were collected, washed once with PBS 1x, snap-frozen in liquid nitrogen and stored at −80 °C until further processing. Each sample used for RNA isolation contained two pooled bi- or tri-partite NSPHs, with a total number of (i) $n = 4$ for unstimulated bi-partite NSPHs (with $n = 4$ biological replicates), (ii) $n = 4$ for stimulated bi-partite NSPHs (with $n = 4$ biological replicates), (iii) $n = 5$ for unstimulated tri-partite NSPHs (with $n = 4$ biological replicates, one sample was sequenced twice), (iv) $n = 5$ for stimulated tri-partite NSPHs (with $n = 4$ biological replicates, one sample was sequenced twice). Post-hoc analysis according to the RNA-Seq sample size estimation method described by Hart et al. (Hart et al., 2013) confirmed a minimum of $n = 4$ to be sufficient to detect 2-fold changes in gene expression for this analysis (see Supplementary File 1 for detailed sample size calculation). Total RNA was isolated using the RNeasy® Mini kit (Qiagen, Benelux, Belgium), according to the manufacturer's protocol. Briefly, 200 μL of chloroform was added to the sample and, after phase separation, RNA was extracted and purified on RNeasy Mini spin columns. The purity and concentration of the RNA samples were evaluated by ultraviolet spectroscopy (NanoDrop, Thermo Scientific, Wilmington, USA). The integrity of the RNA samples was evaluated by the Agilent 4150 TapeStation System using the recommended RNA ScreenTape assay (Agilent Technologies, Inc., Waldbronn, Germany). For all samples, the RNA integrity number (RIN) values were above 7, indicating the superior quality of the isolated RNA. The mRNA library preparation, pair-end transcriptome sequencing, and sequencing data quality control were conducted by Novogene Co., LTD (Cambridge, UK). The data have been deposited with links to BioProject accession number PRJNA989029 in the NCBI BioProject database (https://www.ncbi.nlm.nih.gov/bioproject/).

2.10. Processing of RNA sequencing data

Approximately 20–35 million 150 bp reads were obtained from all samples. After trimming the adapter sequences, low quality bases, and very short reads, the resulting clean reads were aligned to the mouse reference genome Mus_musculus GRCm39 annotated with Ensembl version 106 and STAR 2.7.10b. (Dobin et al., 2013). Quantification of the mapped reads was then performed with the program Featurecounts using the Subread package (Liao et al., 2019). Analysis of differentially expressed genes (DEGs) was performed using the packages DESeq2 (Love et al., 2014) and edgeR (Robinson et al., 2010), implemented in the BigOmics Playground platform (v3.2.2) (Akhmedov et al., 2020). An adjusted p-value $< 0,05$ and an absolute log2 fold change of 1 were defined as significance and expression level cutoffs, respectively.

2.11. Label-free proteomics

Following collection of the cell culture supernatant, individual bi- and tri-partite NSPHs were collected and washed once with PBS, followed by snap-freezing on liquid nitrogen and stored at −80 °C until further processing. For label-free shotgun proteomics analysis, samples were treated according to the FASP (Filter Aided Sample Preparation) protocol. Briefly, 9 NSPHs were pooled for each experimental condition (unstimulated bi-partite, stimulated bipartite, unstimulated tri-partite and stimulated tri-partite). Next, NSPHs were lysed by mechanical homogenization by using a turrax mixer (1-minute, highest speed) and ultrasonication (80 % amplitude, Sonicator U200S control, IKA Labortechnik, Staufen, Germany) on ice in lysis buffer (urea 6 M in 100 mM Tris/HCl, p H = 7,5), followed by centrifugation (1300 rpm) to remove tissue debris. As reported in our previous work (Madonna et al., 2022), a total of 50 μg of protein for each condition were digested with trypsin (0,5 μg/μl Trypsin, Sigma-Aldrich, St. Louis, MI, USA). For protein label-free identification and quantification, 6 μl of tryptic peptides (corresponding to 0,05 μg/ml) from each condition were analysed in triplicate, with an EASY-spray Acclaim™ PepMap™ C18 (75 μm ID, 15 cm L, 2 μm PS, Thermo Fisher Scientific) nanoscale chromatographic column and a total run time of 65 min using a chromatographic gradient from 5 to 90 % of ACN. Proteomics data were acquired with some small changes compared to the protocol initially cited: HCD fragmentation and 240,000 of resolution; the signal intensity threshold was set to 1×10^4 and the MS2 spectra were acquired using a Cycle Time method of 3 s. Precursor ions with charges of + 2 to + 5 were used for MS2 sequencing and scanned in the ion trap by mass tolerance of ± 10 ppm and a m/z scan range of about 300–1200. We performed a HCD fragmentation with a fixed collision energy of 30 % and an activation time of 70 ms. The mass spectrometry proteomics data have been deposited in the ProteomeXchange Consortium via the PRIDE partner repository, with the accession identifier: PXD050649.

2.12. Processing of label-free proteomics data

Proteomics raw data were processed using Thermo Proteome Discoverer (PD) version 2.4.0.305 (Thermo Fischer Scientific) to identify differentially expressed proteins (DEPs) between unstimulated and stimulated bi-partite or tri-partite NSPHs. As "Spectrum Selector", MS^1 precursor was used for the precursor selection within the selected mass-range. Sequest HT was used to search sequence database "uniprot-mouse-proteome-fasta" with maximum missed cleavage sites about 2 and precursor mass tolerance about 10 ppm. In the quantification process, as PD 2.4.0.305 parameters, we selected "Unique + Razor" as peptides to use in the general quantification setting; the precursor abundance quantification was based on the intensity and the normalization was performed on the total peptide amount. Protein abundance was calculated by "Summed abundances"; protein ratios were calculated as "Pairwise Ratio Based" and the statistics hypothesis by t-test was based on background population of proteins or peptides. The univariate statistical analysis was performed to individuate DEPs between two experimental conditions using the "Protein Abundance Ratio" value and the "p-value" for each quantified protein. To perform a robust quantification, we set the parameters "Abundance Ratio Variabilities [%]" less than 50,00 in the ratio, "High identification confidence" for each protein in at least two out of three analytical replicates and the number of "Unique peptides" greater than 1.

2.13. Ingenuity pathway analysis

Obtained DEGs and DEPs lists were uploaded to the Ingenuity Pathway Analysis tool (IPA, Qiagen, Hilden, Germany) to perform a separate gene ontology and functional enrichment analysis using a matrix that contains in each row the quantified protein or gene, the expression ratio and the significance p-value. As such, IPA can predict the activation (z-scores $\geq$ 2,0) or inhibition (z-scores $\leq$ $-$ 2,0) of 'canonical pathways', 'diseases and bio-functions' (downstream pathways) and 'upstream regulators' for the loaded dataset (DEGs or DEPs) based on published literature, as reviewed in Rossi et al., 2022. Additionally, we performed a combined gene ontology and functional enrichment analysis by using a unique global matrix that contains all quantified proteins and genes to characterize stimulated versus unstimulated bi-partite and tri-partite NSPHs.

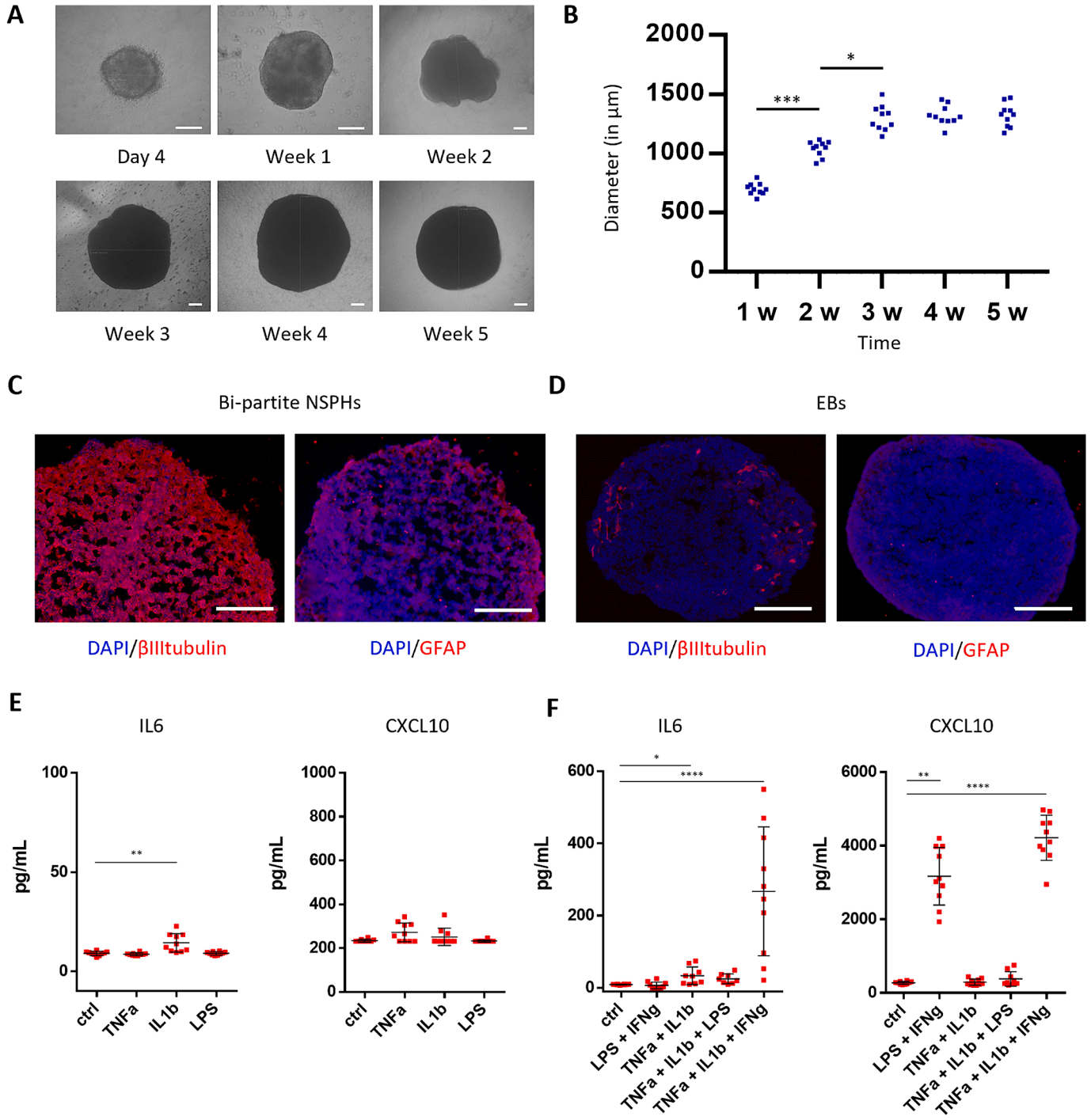

Fig. 2. Growth, characterization and stimulation of bi-partite NSPHs. A) Representative bright-field live cell images of cultured bi-partite NSPHs from week 1 to 5 (Week 1–5). Scale bars: 200 µm. B) Dot plot showing the growth of individual NSPHs over the course of 5 weeks, indicated by the measured diameter (in µm) of the NSPHs (w 1–5, n = 10 each). Representative images of bi-partite NSPHs (C) and EBs (D) immunolabelled for DAPI (blue), β3-tubulin (red) and GFAP (red), as indicated. Scale bars: 100 µm. Dot plots showing IL6 and CXCL10 cytokine secretion (in pg/mL) by bi-partite NSPHs after stimulation with single stimuli (E, n = 10 for each) or combined stimuli (F, n = 10 for each). Abbreviations: w, week; ctrl, unstimulated control. * $p < 0,05$. ** $p < 0,01$. *** $p < 0,001$. **** $p < 0,0001$.

3. Results

3.1. Generation, characterisation and stimulation of bi-partite NSPHs

Bi-partite NSPHs were generated starting from a previously reported $CX_3CR1^{eGFP+/-}$ $CCR2^{RFP+/-}$ C57BL/6 miPSC line (Quarta et al., 2019), as described in detail in the Materials and Methods section. Starting from $2x10^3$ miPSCs, small NSPHs already developed after a few days in culture due to the initial self-assembly capacity of the seeded miPSCs (Fig. 2A). Subsequently, significant continuous growth was observed until they reached a plateau at week 3, as demonstrated by diameter measurements on microscopic bright-field images (Fig. 2B). After 5 weeks of culture, NSPHs were fixed and processed for ICC analysis to confirm neuron and astrocyte differentiation (Fig. 2C). Here we demonstrate that bi-partite NSPHs display the presence of βIII-tubulin$^+$ neurons throughout the whole NSPH, whereas GFAP$^+$ astrocytes are mostly found at the border of the NSPH. To demonstrate the specificity of the antibodies used to confirm neural differentiation, classical EBs derived from the same miPSC-line only stained for a limited number of neurons and astrocytes (Fig. 2D). After establishing bi-partite NSPHs containing both neurons and astrocytes, we aimed to evaluate their immune-responsiveness to inflammatory stimuli based on the secretion of IL6 and CXCL10 after 3 days of stimulation. Here, NSPHs were first stimulated with TNFα, IL1β or LPS as a single stimulus. However, the release of IL6 was, even though significant, only slightly induced in IL1β-treated NSPHs as compared to unstimulated NSPHs, while no significant release of CXCL10 was detected in any of the tested conditions (Fig. 2E). Next, in order to elicit a stronger immune response, multiple stimuli were combined (Fig. 2F). Our results show that the combinations of TNFα + IL1β and TNFα + IL1β + IFNγ were able to significantly induce IL6 release by NSPHs as compared to unstimulated NSPHs, with the combination of TNFα + IL1β + IFNγ being the most efficient. No IL6 secretion was detected when NSPHs were stimulated with LPS + IFNγ. When we analysed the secretion of CXCL10, we observed a significant release of high levels of CXCL10 by NSPHs stimulated with LPS + IFNγ and TNFα + IL1β + IFNγ, as compared to unstimulated NSPHs. Concluding, we here demonstrate the successful generation of bi-partite NSPHs, containing both neurons and astrocytes, that can be triggered to release both IL6 and CXCL10 upon stimulation with TNFα + IL1β + IFNγ. All further analyses described below are performed under this experimental condition.

3.2. Generation, characterisation and stimulation of tri-partite NSPHs

Tri-partite NSPHs were generated from $CX_3CR1^{eGFP+/-}$ $CCR2^{RFP+/-}$ C57BL/6 miPSCs, as described in detail in the Materials and Methods section. Briefly, similar to published protocols for the generation of hiPSC-derived tri-partite NSPHs (Abud et al., 2017; Muffat et al., 2018; Fagerlund et al., 2022), here we relied on the spontaneous migration ability of microglia progenitor cells into developing bi-partite NSPHs. Hereto, 2 x 10^4 $CX_3CR1^{eGFP+/-}$ $CCR2^{RFP+/-}$ C57BL/6 miPSC-derived microglia progenitor cells (Quarta et al., 2019) were added to 2-week-old developing bi-partite NSPHs (see previous section). While $CX_3CR1^{eGFP+/-}$ $CCR2^{RFP+/-}$ C57BL/6 miPSC-derived microglia progenitor cells do not yet express the eGFP reporter protein at this stage of development, as demonstrated in our preceding studies, they express eGFP/CX_3CR1 upon further microglial differentiation in a neural environment (Quarta et al., 2019). Subsequently, their integration into the developing bi-partite NSPHs can be easily monitored by live-cell imaging (Fig. 3A). Already from the third day after addition, amoeboid eGFP$^+$/CX_3CR1^+ microglia clustered in different areas of the NSPHs. Upon further cultivation (2-weeks after seeding), the presence of eGFP$^+$/CX_3CR1^+ microglia increased, and they assumed a ramified shape within the NSPHs. Finally, after a total of 5-weeks of culture (3-weeks after seeding of the microglia progenitors), NSPHs were fixed and processed for ICC analysis to confirm the differentiation of neurons,

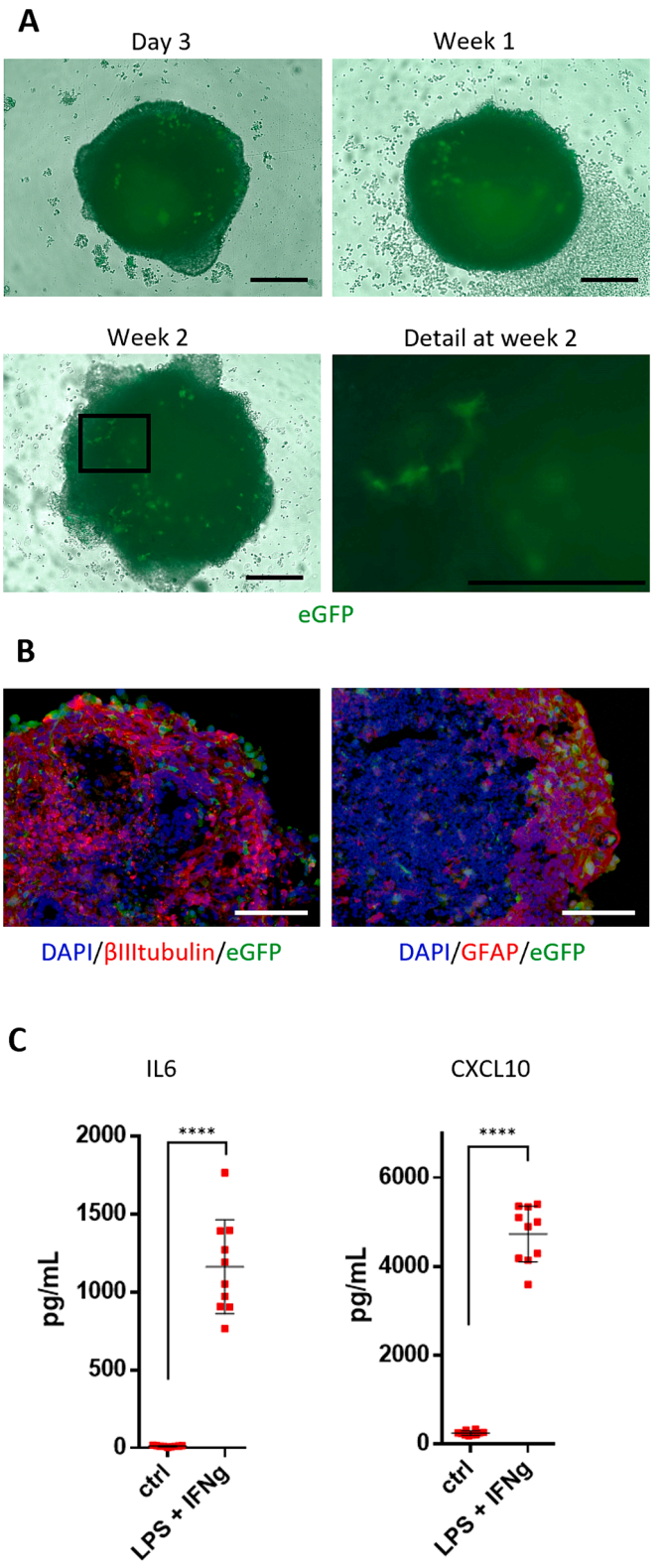

Fig. 3. Characterization and stimulation of tri-partite NSPHs. A) Representative fluorescence live cell images of cultured tri-partite NSPHs on day 3, week 1 and week 2 after addition of microglia progenitor cells to 2-week-old bi-partite NSPHs. eGFP$^+$ microglia in green. Scale bars: 200 μm. (B) Representative images of tri-partite NSPHs immunolabelled for DAPI (blue), βIII-tubulin (red) and GFAP (red) combined with direct eGFP$^+$/CX_3CR1^+ fluorescence (green). Scale bars: 100 μm. (C) Dot plots showing IL6 and CXCL10 cytokine secretion (in pg/mL) by tri-partite NSPHs following stimulation with LPS + IFNγ (n = 10 for each). Abbreviations: ctrl, unstimulated control. **** $p < 0{,}0001$.

astrocytes and microglia (Fig. 3B). Here we confirm that tri-partite NSPHs display the presence of βIII-tubulin$^+$ neurons throughout the whole NSPH, whereas GFAP$^+$ astrocytes and eGFP$^+$ microglia are mostly localized at the outer border of the NSPH. After obtaining tri-partite NSPHs containing neurons, astrocytes and microglia, we also evaluated their immune-responsiveness to inflammatory stimuli based on the secretion of IL6 and CXCL10 after 3 days of stimulation. For this, NSPHs were stimulated with LPS + IFNγ and our results demonstrate significant high release of both IL6 and CXCL10 as compared to unstimulated NSPHs (Fig. 3C). In conclusion, we here demonstrate the successful generation of tri-partite NSPHs, containing neurons, astrocytes and microglia, which can be triggered to release both IL6 and CXCL10 upon stimulation with LPS + IFNγ. All further analyses described below are performed using this experimental condition.

3.3. Stimulated bi-partite and tri-partite NSPHs form stress granules

Given our observation that both bi-partite and tri-partite NSPHs can be subjected to inflammatory stress, as demonstrated by the release of IL6 and CXCL10, we next questioned whether this response is also associated with cellular stress within the NSPHs. Hereto, we investigated the formation of stress granules in bi-partite and tri-partite NSPHs following stimulation with TNFα + IL1β + IFNγ and LPS + IFNγ, respectively. ICC analysis demonstrated the presence of two known protein components of stress granules, namely G3BP1 (G3BP stress granule assembly factor 1) and PABPC1 (poly(A) binding protein cytoplasmic 1) in both bi-partite and tri-partite NSPHs after 3 days of stimulation (Fig. 4). To summarise, we here demonstrate that both bi-partite and tri-partite NSPHs not only secrete pro-inflammatory cytokines upon appropriate stimulation, but more importantly, are also subjected to cellular stress by the formation of stress granules. The latter indicates that multiple cellular processes may be triggered and is investigated further below.

3.4. Canonical pathways affected in stimulated bi-partite and tri-partite NSPHs

Having demonstrated IL6 and CXCL10 production by stimulated bi-partite and tri-partite NSPHs, as well as the subsequent appearance of stress granules, we proceeded with an untargeted transcriptomic and proteomic analysis on control and stimulated bi-partite and tri-partite NSPHs in order to characterize their activation profile in more detail in terms of differentially expressed genes (DEGs) and differentially expressed proteins (DEPs), as described in detail in the Materials and Methods section. Our analyses identified 315 DEGs and 172 DEPs between control and stimulated bi-partite NSPHs, while 5404 DEGs and 130 DEPs were identified between control and stimulated tri-partite NSPHs (supplementary file 2). Subsequently, for Gene Ontology enrichment analysis of bi-partite and tri-partite NSPHs, both DEG and DEP datasets were uploaded together into Qiagen IPA bioinformatics software in order to identify the predicted modulation (up- or down-regulation) of canonical pathways, comprising currently well-characterized metabolic and cell signalling pathways (supplementary file 3). Next, the identified pathways were manually curated based on NSPH-relevant pathways and a significant activation z-score (>2 or < -2 for bi-partite and tri-partite NSPHs). The activation z-score is a statistical value that predicts the activation states of biological functions. This prediction is based on the changes in the expression of a gene or protein of the loaded samples compared to what is expected from literature and describes whether a direction (“increased” or “decreased”) of change is

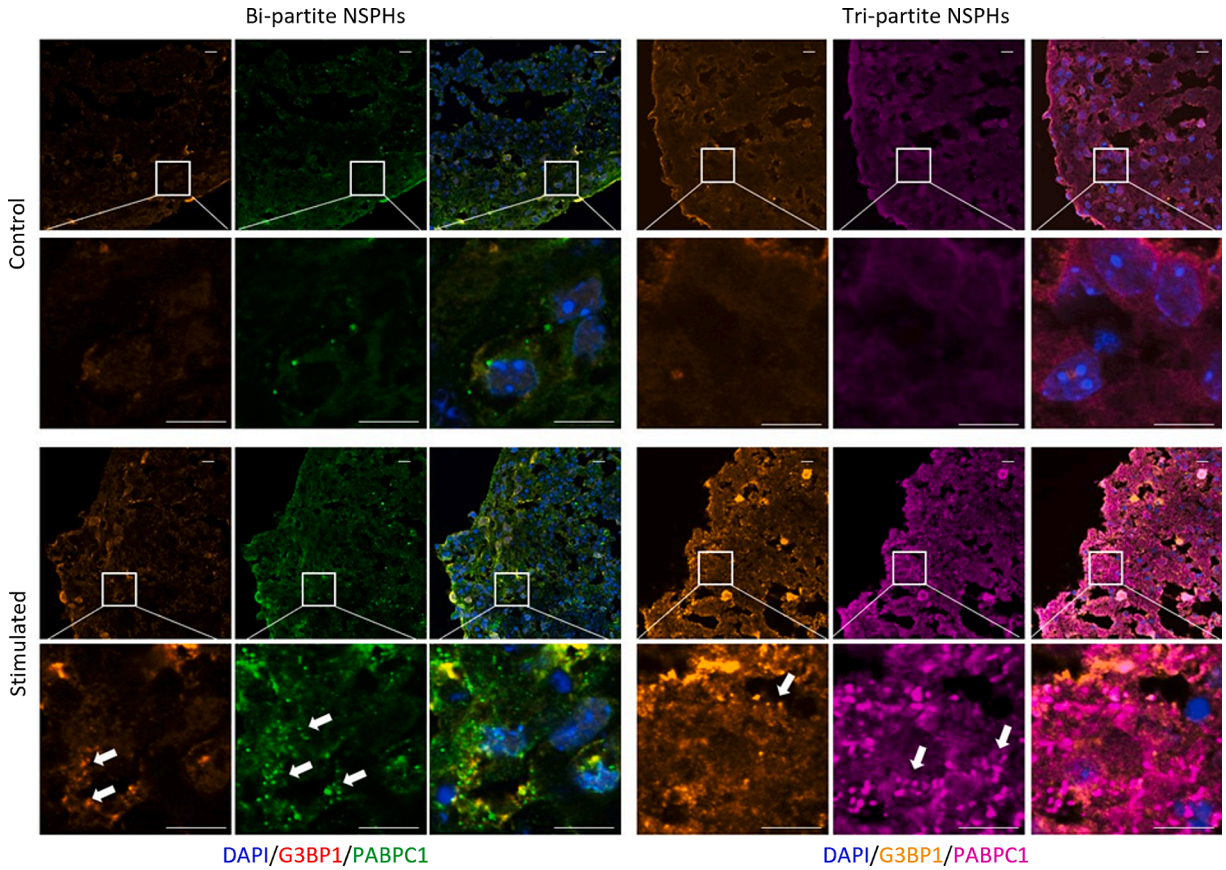

Fig. 4. Formation of stress granules in stimulated bi-partite and tri-partite NSPHs. Representative images of bi-partite NSPHs exposed to TNFα, IL1β and IFNγ (left panels) and tri-partite NSPHs exposed to LPS and IFNγ (right panels) for 72 h, immunolabeled for G3BP1 (orange) and PABPC1 (green-left, magenta-right). White arrows indicate stress granules. Scale bar, 20 μm.

present (Krämer et al., 2014). Subsequently, the remaining signalling pathways were classified into the following four main categories: immune signalling, cell survival, cellular metabolism and neuronal functioning (Fig. 5). Immune signalling pathways are significantly activated following stimulation in both bi-partite and tri-partite NSPHs, with a higher number of pathways activated in tri-partite NSPHs. More specifically, stimulated tri-partite NSPHs show a clear activation of the myeloid TREM1 signalling pathway (https://geneglobe.qiagen.com/us/knowledge/pathways/trem1-signaling), as well as the neuroinflammation signalling pathway (https://geneglobe.qiagen.com/us/knowledge/pathways/neuroinflammation-signaling-pathway). The fact that both are significantly activated in tri-partite NSPHs, but not in bi-partite NSPHs, is most likely a consequence of LPS-stimulated microglia in tri-partite NSPHs. On the other hand, both bi-partite and tri-partite NSPHs display significant activation of the interferon signalling pathway as a consequence of IFNγ being present in the stimulatory cocktails, TNFα + IL1β + IFNγ and LPS + IFNγ respectively. In contrast to tri-partite NSPHs, only the bi-partite NSPHs display a significant activation of the IL1 signalling pathway due to explicit stimulation with IL1β in the stimulatory cocktail. At the level of cell survival, the iNOS signalling pathway is significantly activated in both bi-partite and tri-partite NSPHs, and as such may contribute to cellular apoptosis and/or pyroptosis (see also the next section of Diseases and Biofunctions). Interestingly, in stimulated tri-partite also the necroptosis pathway is significantly activated, which is likely related to cytokine secretion by LPS-stimulated microglia. Furthermore, as a consequence of the occurring inflammatory and cell death processes, there is a marked deregulation of cellular metabolic processes in both bi-partite and tri-partite NSPHs, including cellular energy production, nucleotide and amino acid biosynthesis, as well as cholesterol metabolism. Finally, and most remarkably, stimulated tri-partite NSPHs display significant deactivation of cellular pathways related to neuronal function, which was not observed in stimulated bi-partite NSPHs. Hereby, we conclude that, both bi-partite and tri-partite NSPHs activate multiple canonical pathways upon appropriate stimulation, with a higher number affected in tri-partite NSPHs. These results emphasise the important role and the need to integrate microglia into NSPHs for detailed studies related to inflammation-mediated neurodegeneration.

3.5. *Diseases and biofunctions triggered in stimulated bi-partite and tri-partite NSPHs*

Following analysis of canonical pathways, Qiagen IPA bioinformatics software was also used to predict diseases and biofunctions induced in stimulated bi-partite and tri-partite NSPHs. This analysis predicts the affected biology based on gene/protein expression and predicts the directional change of this effect (supplementary file 4). Diseases and biofunctions can be considered as downstream effects (Krämer et al., 2014). Here, based on the combined DEG and DEP datasets, the obtained diseases and biofunctions were manually curated for NSPH-relevant biology, as well as significant z-scores (>2 or < -2 for bi-partite and tri-partite NSPHs). Next, the remaining diseases and biofunctions were categorized into the following four main subcategories: immune response, viability, homeostasis and development. For visual representation, bubble plots were generated for bi-partite and tri-partite NSPHs, providing z-score, counts and $-\log_{10}$(p-value) (Fig. 6). The counts show the number of proteins and genes involved in each function, reflected in the size of the bubbles (the bigger the bubbles, the higher the number of the counts). The colour of the bubbles represents the significance of the p-value (green has the lowest significance, red the highest), while the grey bubbles have no prediction (all coloured bubbles are significant). Additionally generated bubble plots based on the non-combined DEG and DEP datasets are provided in supplementary Figs. 1 and 2. First, our data analysis indicates significantly increased necrosis, DNA damage and apoptosis, as well as significantly decreased cell survival, in bi-partite NSPHs as a downstream effect of stimulation with TNFα +

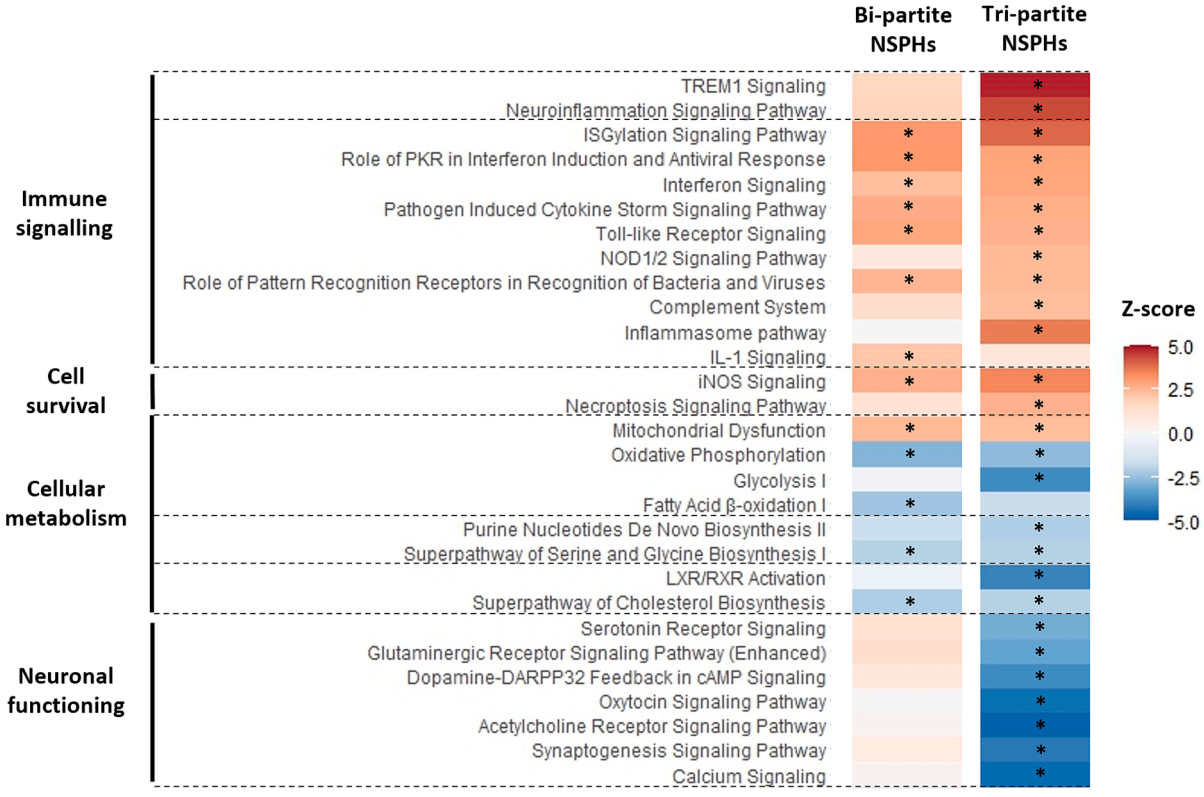

Fig. 5. Canonical pathways affected in stimulated bi-partite and tri-partite NSPHs. Visual representation of the activation z-scores for selected canonical pathways in stimulated bi-partite and tri-partite NSPHs, with colour scaling from 5 (dark red) to −5 (dark blue). Asterisks show significantly affected canonical pathways (z-score > 2 or < -2).

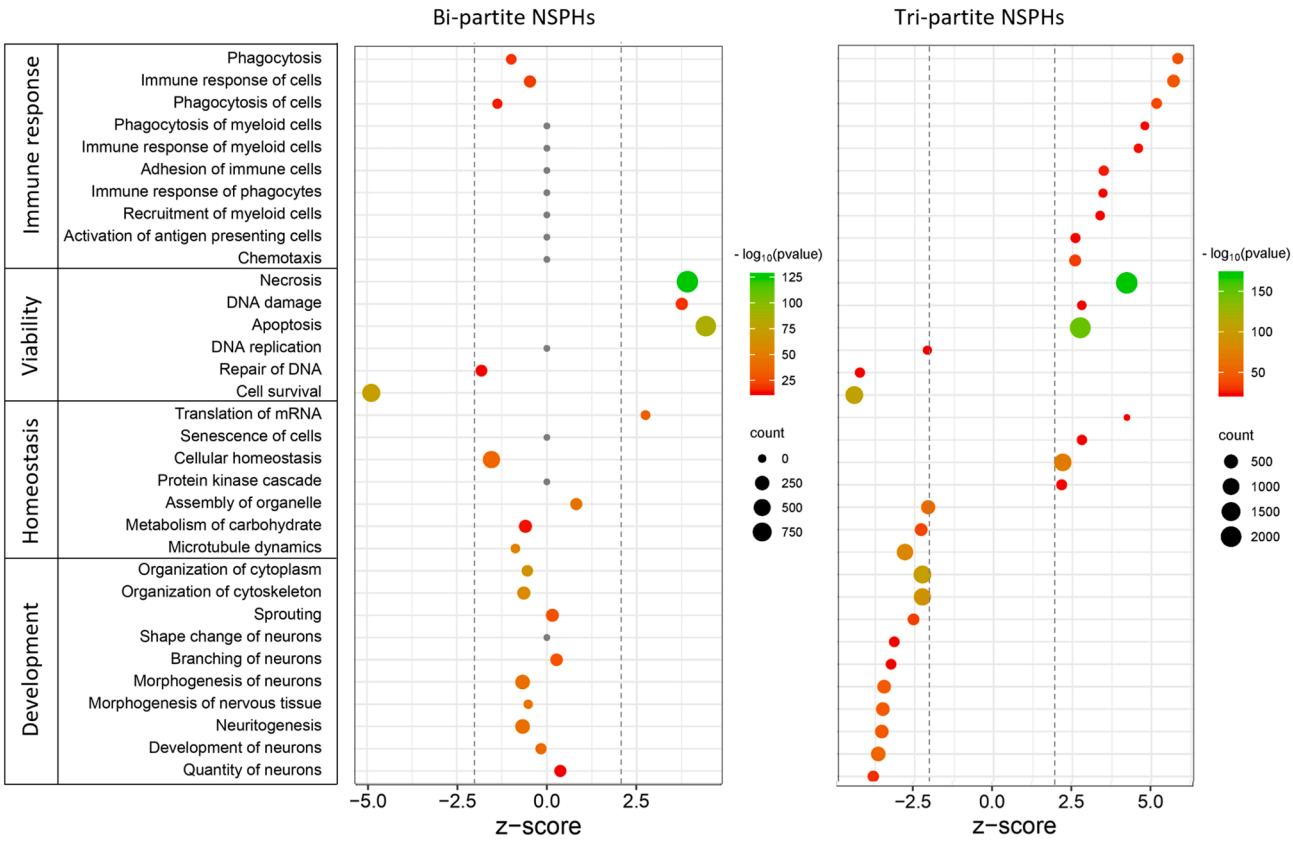

Fig. 6. Diseases and biofunctions triggered in stimulated bi-partite and tri-partite NSPHs based on combined transcriptomic and proteomic analysis. Bubble plot representation of the predicted diseases and biofunctions in stimulated bi-partite and tri-partite NSPHs. A z-score > 2 or < -2 indicates un up- or down-regulation of the activation state of each selected biological function. The colour of the bubbles corresponds to the –log10 p-value (green = most significant) and the size of bubbles refers to the number of gene and protein counts detected within the given biological function.

IL1β + IFNγ (Fig. 6). No significant downstream effects were observed in the subcategories of immune response, homeostasis and development. In contrast, and more interestingly, tri-partite NSPHs display multiple distinct downstream effects as consequence of stimulation with LPS + IFNγ (Fig. 6). Similarly to stimulated bi-partite NSPHs, stimulated tri-partite display significantly increased necrosis, DNA damage and apoptosis, as well as significantly decreased DNA replication, repair of DNA and cell survival. However, stimulated tri-partite NSPHs additionally display significant downstream effects in the subcategories of immune response, homeostasis and development following stimulation with LPS + IFNγ. Most likely as a consequence of microglia stimulation by LPS + IFNγ, significant downstream inflammatory responses, including phagocytosis, chemotaxis and cell adhesion, are detected. Although these downstream inflammatory responses were not observed in bi-partite NSPHs, they also significantly affected cellular homeostasis, including cellular signalling, cellular metabolism and cellular organisation, as well as developmental processes related to neuronal development. Altogether, our combined transcriptomic and proteomic analysis reveals an increased number of significantly activated diseases and biofunctions in stimulated tri-partite NSPHs as compared to stimulated bi-partite NSPHs.

4. Discussion

In previous reports (Quarta et al. 2019 & 2021), we optimized a novel protocol for the differentiation of miPSC-derived microglia progenitor cells. In these studies, eGFP$^-$/CX$_3$CR1$^-$ microglia progenitors were generated from CX$_3$CR1$^{eGFP/-}$CCR2$^{RFP/-}$ C57BL/6 miPSCs, whereby subsequent microglia differentiation could be easily monitored based on eGFP/CX$_3$CR1 expression. As such, we have demonstrated the ability of these eGFP$^-$/CX$_3$CR1$^-$ microglia progenitors to differentiate into ramified eGFP$^+$/CX$_3$CR1$^+$ microglia when co-cultured with astrocyte-committed C57BL/6 embryonic brain-derived neural stem cells (NSC). Further transcriptomic analyses and functional profiling confirmed the microglial identity of the cultured CX$_3$CR1$^{eGFP/-}$CCR2$^{RFP/-}$ C57BL/6 miPSCs derived microglia, and their ability to respond to pro-inflammatory (LPS + IFNγ) and anti-inflammatory (IL13) stimuli. For this new study, we asked ourselves whether the same microglia progenitor cell population would be able to develop into eGFP$^+$/CX$_3$CR1$^+$ microglia when integrated into a 3D environment containing developing neurons and astrocytes (bi-partite NSPHs). Based on the existing literature on generation of microglia-containing hiPSC-derived NSPHs (Abud et al., 2017, Muffat et al., 2018, Fagerlund et al., 2022), we show here a similar co-developmental pattern of miPSC-derived microglia progenitor cells seeded onto developing miPSC-derived bi-partite NSPHs. Following immunocytochemical confirmation of the presence of eGFP$^+$/CX$_3$CR1$^+$ microglia in tri-partite NSPHs (Fig. 3A and 3B), we next assessed the ability of both bi-partite and tri-partite NSPHs to respond to inflammatory stimulation.

At first, upon stimulation with LPS + IFNγ, tri-partite NSPHs significantly released both IL6 and CXCL10 (Fig. 3C), while bi-partite NSPHs released only CXCL10 under the same stimulatory condition (Fig. 2F). These results, in terms of IL6-production, clearly reflect the microglial response to LPS in tri-partite NSPHs. While our preceding studies have shown that LPS stimulation of miPSC-derived astrocytes does not result in detectable IL6 production (Quarta et al., 2019), it cannot be excluded that certain microglia-derived cytokines (upon stimulation) can act on neurons and/or astrocytes (Liddelow et al., 2017, Hyvarinen et al., 2019). This is supported by the observation that bi-partite NSPHs can be triggered to release IL6 upon stimulation with

TNFα + IL1β + IFNγ (Fig. 2F). Hereby, IL1β seems to be the main inducer (Fig. 2G), albeit aided by IFNγ (Fig. 2F). Even though our transcriptomic data on stimulated tri-partite NSPHs indicates an increase in IL1β mRNA (FC 1.5, $p = 0.02$) and TNFα mRNA (FC 3.8, $p < 0.001$) (Supplementary File 2), we were unable to detect these cytokines at the protein level (by proteomics and/or ELISA, respectively Supplementary File 2 and data not shown). However, this does not exclude the possibility that all IL6 produced by tri-partite NSPHs originates from microglia, as a small portion could still originate from astrocytes due to stimulation with very low amounts of IL1β in a concentrated 3D environment, or even other cytokines that remain to be validated from our DEG and DEP analysis (Supplementary File 2). In contrast, both bi-partite and tri-partite NSPHs are readily triggered to release CXCL10 upon stimulation with IFNγ (Fig. 2F and 3C), which is most likely mediated by astrocytes (Michlmayr et al., 2013). Nevertheless, the stimulatory conditions applied to both bi-partite and tri-partite NSPHs were sufficient to activate a cytokine response.

Given the observation that bi-partite and tri-partite NSPHs were able to respond to inflammatory stimuli, we next investigated whether this response triggers an early stress response. For this, immunocytochemical staining was performed to detect the presence of stress granules. The formation of stress granules is a stress-induced process whereby over 140 cytoplasmic proteins can intertwine with cytoplasmic mRNAs, translation initiation components and proteins affecting mRNA function. In the initial stage of the stress granules formation, it is assumed that they have a protective function, as they enable the cell to control energy expenditure in favour of cell survival. Upon stress withdrawal, stress granules usually disassemble, and normal cellular metabolism and function returns (Motaln et al., 2020). In this study, we demonstrate that stress granules, which can be identified by staining for G3BP1$^+$ and/or PABPC1$^+$ cytoplasmatic aggregates, are still present in both bi-partite and tri-partite NSPHs at day 3 of stimulation (Fig. 4), indicating that NSPHs are under chronic stress at this stage. No complete overlap of G3BP1 and PABPC1 was observed, suggesting that different types of stress granules form and persist in NSPHs. It may thus be hypothesised that increased formation or reduced clearance of stress granules in both bi-partite and tri-partite NSPHs following pro-inflammatory stimulation could lead to the activation of cell death processes, as is the case in the pathogenesis of many neurodegenerative diseases.

Subsequently, we performed an untargeted transcriptomic and proteomic analysis to identify downstream cellular processes as a consequence of the observed inflammation-induced stress response. By performing both transcriptomics and proteomics, we aimed to rule out potential bias based on the common knowledge that mRNA transcription does not always reflect protein translation, and *vice versa*. As such, by combining both datasets for canonical pathway analysis and downstream biofunctions and diseases (Figs. 5 and 6), the obtained analyses suggest that tri-partite NSPHs seem to suffer more severely than bi-partite NSPHs after pro-inflammatory stimulation. To further investigate this observation, we performed flow cytometric analysis on dissociated unstimulated and stimulated bi-partite and tri-partite NSPHs to determine actual cell death. Although we do not fully understand the reason, flow cytometric analysis revealed no evidence of decreased cell survival in both bi-partite and tri-partite NSPHs upon pro-inflammatory stimulation (data not shown). However, there may be several explanations for this. Firstly, the dissociation process applied may have influenced this outcome, with dead or dying cells being disrupted and as such excluded from further analysis. Secondly, and more likely, given the time point of analysis (72 h of stimulation), cells may have activated the cell death processes, but have not yet reached the stage of actual cell death. This warrants us to perform longitudinal studies in our future research that may extend up to weeks after pro-inflammatory stimulation.

With regard to our combined transcriptomic and proteomic analysis, it is important to note that IPA analysis could only predict highly significant upstream regulators when both DEGs and DEPs were combined into a single analysis. Based on the experimental outcome, IPA identified TNFα, IL1β and IFNγ as the main upstream regulators for the observed transcriptomic and proteomic changes in stimulated bi-partite NSPHs, whereas LPS and IFNγ were identified for stimulated tri-partite NSPHs (Supplementary File 5). This further confirms that the canonical pathways, as well as the diseases and biofunctions identified in stimulated bi-partite and tri-partite NSPHs are directly linked to the inflammatory stimulation provided. We expect that a combination of transcriptomics and proteomics may become a standard tool for analysing complex signalling alterations in bi-partite and tri-partite NSPHs, and to an even greater extent in more complex organoids that include oligodendrocytes and endothelial cells. However, we do want to mention that besides the combined analysis, individual transcriptomic and proteomic analyses should also be performed and compared with the combined analysis. For example, while chemotaxis was clearly identified among the diseases and biofunctions for both bi-partite and tri-partite NSPHs when analysing only the DEGs (Supplementary File 4 and Supplementary Fig. 1), it was not identified when analysing only the DEPs for both bi-partite and tri-partite NSPHs (Supplementary File 4 and Supplementary Fig. 2). Overall, combined analysis rather suggests that chemotaxis is only significant in tri-partite NSPHs, but not in bi-partite NSPHs, which may need further follow up functional validation (Fig. 6). As such, it was shown that both bi-partite and tri-partite NSPHs effectively produce CXCL10 upon stimulation (Figs. 2 and 3). However, this discrepancy can be explained by the fact that proteomics analysis was performed on the NSPHs, but not on the culture medium, and as such, secreted cytokines were not readily detected.

Finally, we want to highlight that this is to our best knowledge, the first study to perform a combined transcriptomic and proteomic analysis of murine iPSC-derived bi-partite and tri-partite NSPHs upon inflammatory stimulation. By doing so, we have identified multiple affected signalling pathways, especially in microglia-containing tri-partite NSPHs, that will be of utmost importance for future NSPH research by us and others. For example, being highly activated in tri-partite NSPHs, the further functional analysis of individual genes and proteins contributing to the TREM1 and neuro-inflammation signalling pathway, will even further increase our understanding of inflammation-induced cellular distress and function in NSPHs (see supplementary Figs. 3 and 4 for the TREM1 signalling pathway in bipartite and tripartite NSPHs, respectively, and supplementary Figs. 5 and 6 for the neuroinflammation signalling pathway in bipartite and tripartite NSPHs, respectively). Additionally, and maybe not unexpectedly, stimulated tri-partite NSPHs appear to suffer from a high distortion in neuronal development or function (Fig. 5). Although not the purpose of this study, one such future direction is the implementation of novel technologies to measure electrophysiological activity in miPSC-derived NSPHs. Even though preliminary in nature, further ICC analyses already confirmed the presence of the presynaptic marker synaptophysin in both bi-partite and tri-partite NSPHs, indicating the possibility to make functional neuronal connections (Supplementary Fig. 7). Obviously, this part will need further quantification, as well as validation using ICC for post-synaptic markers in order to unravel the role of incorporated microglia on neuronal network development in tri-partite NSPHs, as well as the role of microglial inflammatory response on NSPH electrophysiological behaviour. Once those techniques have been fully established, NSPH analysis will become fully multi-modal and multi-omics, aiming at deep cellular, molecular and functional interrogation of inflammatory signalling in an *in vitro* neural-like context.

5. Conclusions

In this study we have presented optimised culture conditions for bi-partite and tri-partite miPSC-derived NSPHs that can be subjected to cellular stress upon appropriate activation. By combining untargeted transcriptomic and proteomic analysis of bi-partite and tri-partite NSPHs, we have demonstrated that the presence of microglia in

NSPHs results in a robust immune response and exacerbates cellular stress processes.

CRediT authorship contribution statement

Julia Di Stefano: Writing – review & editing, Writing – original draft, Methodology, Investigation, Formal analysis, Conceptualization. **Laura Garcia-Pupo:** Writing – review & editing, Methodology, Investigation, Formal analysis. **Federica Di Marco:** Writing – review & editing, Methodology, Investigation, Formal analysis. **Helena Motaln:** Writing – review & editing, Writing – original draft, Resources, Methodology, Investigation, Formal analysis. **Jonas Govaerts:** Investigation, Formal analysis. **Elise Van Breedam:** Methodology. **Ligia Monica Mateiu:** Methodology. **Siebe Van Calster:** Investigation. **Leonardo Ricciardi:** Formal analysis. **Alessandra Quarta:** Methodology. **Peter Verstraelen:** Writing – review & editing, Writing – original draft, Supervision, Resources, Methodology, Funding acquisition, Conceptualization. **Winnok H. De Vos:** Resources. **Boris Rogelj:** Resources. **Ilaria Cicalini:** Methodology. **Vincenzo De Laurenzi:** Resources, Funding acquisition. **Piero Del Boccio:** Resources. **Una FitzGerald:** Conceptualization, Funding acquisition. **Wim Vanden Berghe:** Supervision, Methodology. **Marleen Verhoye:** Supervision, Funding acquisition. **Damiana Pieragostino:** Supervision, Resources, Methodology, Funding acquisition, Conceptualization. **Peter Ponsaerts:** Writing – review & editing, Writing – original draft, Supervision, Resources, Methodology, Funding acquisition, Conceptualization.

Declaration of Competing Interest

The authors declare that they have no known competing financial interests or personal relationships that could have appeared to influence the work reported in this paper.

Data availability

Data will be made available on request.

Acknowledgement and funding sources

This research and the PhD fellowship of JDS were funded by the European Union's Horizon 2020 research and innovation programme under the Marie Skłodowska-Curie grant agreement No 813263 (PMSMatTrain, granted to UF, PP, MVH, DP and VDL). Additional support was provided by the Fund for Scientific Research Flanders (FWO-Vlaanderen) of the Flemish Government (FWO research project G091518N and FWO sabbatical bench fee K800224N, both granted to PP; Short Research Stay in Flanders V511123N, granted to HM; FWO research projects I000123N and I003420N, granted to WDV), the Slovenia Research and Innovation Agency (P4-0127, J3-3065 granted to BR), the 'Bijzonder Onderzoeksfonds' (BOF) MSCA grant #47375 TRANS4AD granted to LG and BOF of the University of Antwerp, Belgium (UA BOF-GOA 2020, UA BOF-SEP 2022 and BOF Research Sabbatical 2023, all granted to PP). We also acknowledge support from the SAO-FRA grant 20230041 (Stichting Alzheimer Onderzoek - Belgium, granted to WDV and PV).

Appendix A. Supplementary data

Supplementary data to this article can be found online at https://doi.org/10.1016/j.bbi.2024.07.008.

References

Abreu, C.M., Gama, L., Krasemann, S., Chesnut, M., Odwin-Dacosta, S., Hogberg, H.T., Hartung, T., Pamies, D., 2018. microglia increase inflammatory responses in iPSC-derived human brainspheres. Front Microbiol. 4 (9), 2766, 10.3389/fmicb.2018.02766. PMID: 30619100; PMCID: PMC6296317.

Abud, E.M., Ramirez, R.N., Martinez, E.S., Healy, L.M., Nguyen, C.H.H., Newman, S.A., Yeromin, A.V., Scarfone, V.M., Marsh, S.E., Fimbres, C., Caraway, C.A., Fote, G.M., Madany, A.M., Agrawal, A., Kayed, R., Gylys, K.H., Cahalan, M.D., Cummings, B.J., Antel, J.P., Mortazavi, A., Carson, M.J., Poon, W.W., Blurton-Jones, M., 2017. iPSC-derived human microglia-like cells to study neurological diseases. Neuron. 94 (2), 278–293.e9. https://doi.org/10.1016/j.neuron.2017.03.042. PMID: 28426964; PMCID: PMC5482419.

Akhmedov M, Martinelli A, Geiger R, Kwee I. Omics Playground: a comprehensive self-service platform for visualization, analytics and exploration of Big Omics Data. NAR Genom Bioinform. 2019 Dec 6;2(1):lqz019. doi: 10.1093/nargab/lqz019. PMID: 33575569; PMCID: PMC7671354.

DiSabato DJ, Quan N, Godbout JP. Neuroinflammation: the devil is in the details. J Neurochem. 2016 Oct;139 Suppl 2(Suppl 2):136-153. doi: 10.1111/jnc.13607. Epub 2016 May 4. PMID: 26990767; PMCID: PMC5025335.

Dobin A, Davis CA, Schlesinger F, Drenkow J, Zaleski C, Jha S, Batut P, Chaisson M, Gingeras TR. STAR: ultrafast universal RNA-seq aligner. Bioinformatics. 2013 Jan 1; 29(1):15-21. doi: 10.1093/bioinformatics/bts635. Epub 2012 Oct 25. PMID: 23104886; PMCID: PMC3530905.

Fagerlund, I., Dougalis, A., Shakirzyanova, A., Gómez-Budia, M., Pelkonen, A., Konttinen, H., Ohtonen, S., Fazaludeen, M.F., Koskuvi, M., Kuusisto, J., Hernández, D., Pebay, A., Koistinaho, J., Rauramaa, T., Lehtonen, Š., Korhonen, P., Malm, T., 2021. Microglia-like cells promote neuronal functions in cerebral organoids. Cells. 11 (1), 124. https://doi.org/10.3390/cells11010124. PMID: 35011686; PMCID: PMC8750120.

Fan, P., Wang, Y., Xu, M., Han, X., Liu, Y., 2022. The application of brain organoids in assessing neural toxicity. Front Mol Neurosci. 9 (15), 799397 https://doi.org/10.3389/fnmol.2022.799397. PMID: 35221913; PMCID: PMC8864968.

Hart SN, Therneau TM, Zhang Y, Poland GA, Kocher JP. Calculating sample size estimates for RNA sequencing data. J Comput Biol. 2013 Dec;20(12):970-8. doi: 10.1089/cmb.2012.0283. Epub 2013 Aug 20. PMID: 23961961; PMCID: PMC3842884.

Hyvärinen, T., Hagman, S., Ristola, M., Sukki, L., Veijula, K., Kreutzer, J., Kallio, P., Narkilahti, S., 2019. Co-stimulation with IL-1β and TNF-α induces an inflammatory reactive astrocyte phenotype with neurosupportive characteristics in a human pluripotent stem cell model system. Sci Rep. 9 (1), 16944, 10.1038/s41598-019-53414-9. PMID: 31729450; PMCID: PMC6858358.

Jin M, Xu R, Wang L, Alam MM, Ma Z, Zhu S, Martini AC, Jadali A, Bernabucci M, Xie P, Kwan KY, Pang ZP, Head E, Liu Y, Hart RP, Jiang P. Type-I-interferon signaling drives microglial dysfunction and senescence in human iPSC models of Down syndrome and Alzheimer's disease. Cell Stem Cell. 2022 Jul 7;29(7):1135-1153.e8. doi: 10.1016/j.stem.2022.06.007. PMID: 35803230; PMCID: PMC9345168.

Krämer A, Green J, Pollard J Jr, Tugendreich S. Causal analysis approaches in Ingenuity Pathway Analysis. Bioinformatics. 2014 Feb 15;30(4):523-30. doi: 10.1093/bioinformatics/btt703. Epub 2013 Dec 13. PMID: 24336805; PMCID: PMC3928520.

Lancaster MA, Knoblich JA. Organogenesis in a dish: modeling development and disease using organoid technologies. Science. 2014 Jul 18;345(6194):1247125. doi: 10.1126/science.1247125. Epub 2014 Jul 17. PMID: 25035496.

Liao, Y., Smyth, G.K., Shi, W., 2019. The R package Rsubread is easier, faster, cheaper and better for alignment and quantification of RNA sequencing reads. Nucleic Acids Res. 47 (8), 10.1093/nar/gkz114. PMID: 30783653; PMCID: PMC6486549 e47.

Liddelow SA, Guttenplan KA, Clarke LE, Bennett FC, Bohlen CJ, Schirmer L, Bennett ML, Münch AE, Chung WS, Peterson TC, Wilton DK, Frouin A, Napier BA, Panicker N, Kumar M, Buckwalter MS, Rowitch DH, Dawson VL, Dawson TM, Stevens B, Barres BA. Neurotoxic reactive astrocytes are induced by activated microglia. Nature. 2017 Jan 26;541(7638):481-487. doi: 10.1038/nature21029. Epub 2017 Jan 18. PMID: 28099414; PMCID: PMC5404890.

Lin YT, Seo J, Gao F, Feldman HM, Wen HL, Penney J, Cam HP, Gjoneska E, Raja WK, Cheng J, Rueda R, Kritskiy O, Abdurrob F, Peng Z, Milo B, Yu CJ, Elmsaouri S, Dey D, Ko T, Yankner BA, Tsai LH. APOE4 Causes Widespread Molecular and Cellular Alterations Associated with Alzheimer's Disease Phenotypes in Human iPSC-Derived Brain Cell Types. Neuron. 2018 Jun 27;98(6):1141-1154.e7. doi: 10.1016/j.neuron.2018.05.008. Epub 2018 May 31. Erratum in: Neuron. 2018 Jun 27;98 (6): 1294. PMID: 29861287; PMCID: PMC6023751.

Love, M.I., Huber, W., Anders, S., 2014. Moderated estimation of fold change and dispersion for RNA-seq data with DESeq2. Genome Biol. 15 (12), 550, 10.1186/s13059-014-0550-8. PMID: 25516281; PMCID: PMC4302049.

Madonna R, Pieragostino D, Cufaro MC, Del Boccio P, Pucci A, Mattii L, Doria V, Cadeddu Dessalvi C, Zucchi R, Mercuro G, De Caterina R. Sex-related differential susceptibility to ponatinib cardiotoxicity and differential modulation of the Notch1 signalling pathway in a murine model. J Cell Mol Med. 2022 Mar;26(5):1380-1391. doi: 10.1111/jcmm.17008. Epub 2022 Feb 5. PMID: 35122387; PMCID: PMC8899159.

Michlmayr, D., McKimmie, C., 2014. Role of CXCL10 in central nervous system inflammation. Int. J. Interferon, Cytokine Mediator Res. 6, 1–18. https://doi.org/10.2147/IJICMR.S35953.

Motaln, H., Čerček, U., Recek, N., Bajc Česnik, A., Mozetič, M., Rogelj, B., 2020. Cold atmospheric plasma induces stress granule formation via an eIF2α-dependent pathway. Biomater Sci. 8 (19), 5293–5305. https://doi.org/10.1039/d0bm00488j. Epub 2020 Sep 15 PMID: 32930691.

Muffat J, Li Y, Omer A, Durbin A, Bosch I, Bakiasi G, Richards E, Meyer A, Gehrke L, Jaenisch R. Human induced pluripotent stem cell-derived glial cells and neural progenitors display divergent responses to Zika and dengue infections. Proc Natl Acad Sci U S A. 2018 Jul 3;115(27):7117-7122. doi: 10.1073/pnas.1719266115. Epub 2018 Jun 18. PMID: 29915057; PMCID: PMC6142255.

Quarta, A., Le Blon, D., D'aes, T., Pieters, Z., Hamzei Taj, S., Miró-Mur, F., Luyckx, E., Van Breedam, E., Daans, J., Goossens, H., Dewilde, S., Hens, N., Pasque, V.,

Planas, A.M., Hoehn, M., Berneman, Z., Ponsaerts, P., 2019. Murine iPSC-derived microglia and macrophage cell culture models recapitulate distinct phenotypical and functional properties of classical and alternative neuro-immune polarisation. Brain Behav Immun. 82, 406–421. https://doi.org/10.1016/j.bbi.2019.09.009. Epub 2019 Sep 13 PMID: 31525508.

Quarta, A., Meese, T., Pieters, Z., Van Breedam, E., Le Blon, D., Van Broeckhoven, J., Hendrix, S., Goossens, H., Hens, N., Berneman, Z., Van Nieuwerburgh, F., Ponsaerts, P., 2021. Murine induced pluripotent stem cell-derived neuroimmune cell culture models emphasize opposite immune-effector functions of interleukin 13-primed microglia and macrophages in terms of neuroimmune toxicity. Glia. 69 (2), 326–345. https://doi.org/10.1002/glia.23899. Epub 2020 Aug 31 PMID: 32865285.

Renner, H., Grabos, M., Becker, K.J., Kagermeier, T.E., Wu, J., Otto, M., Peischard, S., Zeuschner, D., TsyTsyura, Y., Disse, P., Klingauf, J., Leidel, S.A., Seebohm, G., Schöler, H.R., Bruder, J.M., 2020. A fully automated high-throughput workflow for 3D-based chemical screening in human midbrain organoids. PMID: 33138918; PMCID: PMC7609049 Elife. 3 (9), e52904.

Robinson MD, McCarthy DJ, Smyth GK. edgeR: a Bioconductor package for differential expression analysis of digital gene expression data. Bioinformatics. 2010 Jan 1;26 (1):139-40. doi: 10.1093/bioinformatics/btp616. Epub 2009 Nov 11. PMID: 19910308; PMCID: PMC2796818.

Rossi, C., Cicalini, I., Cufaro, M.C., et al., 2022. Breast cancer in the era of integrating "Omics" approaches. Oncogenesis 11, 17. https://doi.org/10.1038/s41389-022-00393-8.

Sabate-Soler S, Nickels SL, Saraiva C, Berger E, Dubonyte U, Barmpa K, Lan YJ, Kouno T, Jarazo J, Robertson G, Sharif J, Koseki H, Thome C, Shin JW, Cowley SA, Schwamborn JC. Microglia integration into human midbrain organoids leads to increased neuronal maturation and functionality. Glia. 2022 Jul;70(7):1267-1288. doi: 10.1002/glia.24167. Epub 2022 Mar 9. PMID: 35262217; PMCID: PMC9314680.

Samudyata, Oliveira AO, Malwade S, Rufino de Sousa N, Goparaju SK, Gracias J, Orhan F, Steponaviciute L, Schalling M, Sheridan SD, Perlis RH, Rothfuchs AG, Sellgren CM. SARS-CoV-2 promotes microglial synapse elimination in human brain organoids. Mol Psychiatry. 2022 Oct;27(10):3939-3950. doi: 10.1038/s41380-022-01786-2. Epub 2022 Oct 5. PMID: 36198765; PMCID: PMC9533278.

Van Breedam E, Nijak A, Buyle-Huybrecht T, Di Stefano J, Boeren M, Govaerts J, Quarta A, Swartenbroekx T, Jacobs EZ, Menten B, Gijsbers R, Delputte P, Alaerts M, Hassannia B, Loeys B, Berneman Z, Timmermans JP, Jorens PG, Vanden Berghe T, Fransen E, Wouters A, De Vos WH, Ponsaerts P. Luminescent Human iPSC-Derived Neurospheroids Enable Modeling of Neurotoxicity After Oxygen-glucose Deprivation. Neurotherapeutics. 2022 Mar;19(2):550-569. doi: 10.1007/s13311-022-01212-z. Epub 2022 Mar 14. Erratum in: Neurotherapeutics. 2022 Jun 21;: PMID: 35289376; PMCID: PMC9226265.

Xu R, Boreland AJ, Li X, Erickson C, Jin M, Atkins C, Pang ZP, Daniels BP, Jiang P. Developing human pluripotent stem cell-based cerebral organoids with a controllable microglia ratio for modeling brain development and pathology. Stem Cell Reports. 2021 Aug 10;16(8):1923-1937. doi: 10.1016/j.stemcr.2021.06.011. Epub 2021 Jul 22. PMID: 34297942; PMCID: PMC8365109.